PHYSICAL REVIEW D VOLUME 24, NUMBER 12 15 DECEMBER 1981

Nonrelativistic bound states of the non-Abelian gauge potential

R. Vilela Mendes
CFMC-Instituto Nacional de Investigação Científica, Avenida Gama Pinto, 2-1699 Lisboa, Codex, Portugal
(Received 22 December 1980)

The bound-state problem for the nonlocal potential $[c_1 + c_2\cos(\zeta v_r)]/r$ is studied. Exact S-wave solutions are obtained, which behave logarithmically at the origin, and a second-order (parabolic) approximation is used to study higher partial waves.

I. INTRODUCTION

In Ref. 1 the leading large-time behavior of the canonical gauge-theory Hamiltonian was studied. In particular the kernel (in the interaction picture) for the static interaction between two currents, in the center-of-mass frame and when global gauge symmetry is conserved was found to be

$$K(p,q)=\frac{1}{v_r|t|}[c_1+c_2\cos(\zeta v_r)], \tag{1.1}$$

where v_r is the relative velocity $v_r=|\vec{v}_p-\vec{v}_q|$. From this kernel one infers the effective potential between two charged states in the center-of-mass frame

$$V_{\text{c.m.}}=\frac{1}{r}[c_1+c_2\cos(\zeta v_r)]. \tag{1.2}$$

The constants c_1 and c_2 depend on the gauge group: $c_1=1$, $c_2=0$ for U(1); $c_1=\frac{1}{3}$, $c_2=\frac{2}{3}$ for SU(2); $c_1=c_2=\frac{1}{2}$ for SU(3). The nonlocal $\cos(\zeta v_r)$ sums the long-range effects of charged soft gluons. The magnitude of the constant ζ depends on the infrared realization mode and when using (1.2) as a phenomenological potential it should be taken as a free parameter. With the overall coupling constant that multiplies (1.2) the gauge potential has two free parameters in the non-Abelian case.

The technique used in Ref. 1 to obtain the static kernels involves canonical quantization around the trivial vacuum configuration $\vec{A}=0$ and large-time asymptotic expansions in the interaction picture. It is therefore possible that at large distances the non-Abelian gauge potential might still become modified into a confining potential. This might occur by topological effects or even by higher-order dynamical effects (not accessible in a leading-order asymptotic expansion) leading, for example, to pair condensation. The basic claim, therefore, is merely that (1.2) is the correct intermediate-range non-Abelian potential that in phenomenological applications should replace the Coulomb part, usually believed to represent the (nonconfining) gluon exchange contribution.

As a first step towards testing the usefulness of the potential the properties of its nonrelativistic bound states are discussed here. A general technique to deal with this nonlocal problem is developed in Sec. II, whereby the S-wave exact solutions are obtained. The behavior at the origin of the S waves is derived in Sec. IV and in Sec. III a parabolic approximation to the potential is studied which is useful for higher partial waves. Finally in Sec. V the possible relevance of the results to quarkonium systems is briefly discussed.

Although this subject is not studied here, one should point out that the non-Abelian potential may also give rise to interesting effects in the scattering states. For example, there will be "scattering windows" of free wave propagation whenever the relative velocity is such that $c_1+c_2\cos(\zeta v_r)=0$.

II. BOUND STATES: EXACT SOLUTIONS

The Schrödinger equation

$$\left\{-\frac{\hbar}{2m}\nabla^2-\frac{g^2}{r}\left[c_1+c_2\cos\left(\zeta\left(\frac{-\hbar^2\nabla^2}{m^2}\right)^{1/2}\right)\right]\right\}\psi(\vec{x})=E\psi(\vec{x}) \tag{2.1}$$

after separation of the angular variables

$$\psi(\vec{x})=\frac{F_l(r)}{r}\,Y_l^m(\theta,\phi)$$

leads to the following nonlocal radial equation:

$$\left\{-\frac{\hbar^2}{2m}\left(\frac{d^2}{dr^2}-\frac{l(l+1)}{r^2}\right)-\frac{g^2}{r}\left[c_1+c_2\cos\left(\frac{\zeta h}{m}\left(-\frac{d^2}{dr^2}+\frac{l(l+1)}{r^2}\right)^{1/2}\right)\right]\right\}F_l(r)=EF_l(r). \tag{2.2}$$

Let $E<0$ (bound state) and

$$\rho=\frac{(8m|E|)^{1/2}}{\hbar}r,\quad \lambda=\frac{g^2}{\hbar}\left(\frac{m}{2|E|}\right)^{1/2},\quad \xi=\zeta\left(\frac{8|E|}{m}\right)^{1/2}. \tag{2.3}$$

Then Eq. (2.2) becomes

$$\left\{\left(\frac{d^2}{d\rho^2}-\frac{l(l+1)}{\rho^2}\right)+\frac{\lambda}{\rho}\left[c_1+c_2\cos\left(\xi\left(-\frac{d^2}{d\rho^2}+\frac{l(l+1)}{\rho^2}\right)^{1/2}\right)\right]\right\}F_l(\rho)=\tfrac{1}{4}F_l(\rho). \tag{2.4}$$

The bound-state wave functions are the square-integrable solutions to (2.4), satisfying the boundary condition $F_l(0)=0$.

The problem of solving the nonlocal equation (2.4) is reduced to a problem in ordinary differential equations by the use of a Fourier-Hankel transform

$$F_l(\rho)=\int_{-\infty}^{\infty}\alpha\rho h_l^{(+)}(\alpha\rho)\phi_l(\alpha)d\alpha, \tag{2.5}$$

where $h_l^{(+)}$ is a spherical Hankel function of the first kind:

$$h_l^{(+)}(x)=\sum_{s=0}^{l}\frac{i^{s-l}}{2^s s!}\frac{(l+s)!}{(l-s)!}x^{-(s+1)}e^{ix}. \tag{2.6}$$

The transform (2.5) and the radial equation (2.4) then yield

$$\int d\alpha\{\rho(\alpha^2+\tfrac{1}{4})-\lambda[c_1+c_2\cos(\xi\alpha)]\}\times\phi_l(\alpha)\alpha\rho h_l^{(+)}(\alpha\rho)=0,$$

and with (2.6) one derives an ordinary differential equation for each $\phi_l(\alpha)$:

$$\sum_{s=0}^{l}\frac{(l+s)!}{2^s s!(l-s)!}\frac{d^{l-s}}{d\alpha^{l-s}}\left\{i\frac{d}{d\alpha}[\alpha^{-s}(\alpha^2+\tfrac{1}{4})\phi_l]-\lambda\alpha^{-s}[c_1+c_2\cos(\xi\alpha)]\phi_l\right\}=0. \tag{2.7}$$

Equation (2.7) is of order $(l+1)$ and for high l values becomes quite involved. This is the price one pays to convert a nonlocal equation into a problem in ordinary differential equations. The exact solution to Eq. (2.7) will be found for $l=0$ but to estimate level splittings for different orbital angular momenta an approximation to Eq. (2.4) will be used instead of (2.7).

S states. For $l=0$ Eq. (2.7) is

$$i(\alpha^2+\tfrac{1}{4})\frac{d\phi}{d\alpha}+i2\alpha\phi-\lambda[c_1+c_2\cos(\xi\alpha)]\phi=0$$

with solution

$$\phi(\alpha)=\frac{K}{\alpha^2+\frac{1}{4}}\exp\left\{-i\left[2\lambda c_1\tan^{-1}(2\alpha)+\lambda c_2\int^{\alpha}\frac{\cos(\xi y)}{y^2+\frac{1}{4}}dy\right]\right\}.$$

Substitution into (2.5) and a change of variables leads to

$$F_{\lambda,\xi}(\rho)=\frac{\sqrt{2}}{\pi}\int_0^{\pi/2}d\phi\cos\left[\frac{\rho}{2}\tan\phi-2\lambda c_1\phi-2\lambda c_2\int_0^{\phi}\cos\left(\frac{\xi}{2}\tan\phi'\right)d\phi'\right]. \tag{2.8}$$

This is the integral representation of a general exact solution to (2.4) for $l=0$. This function will be a bound-state wave function only when the boundary condition at $\rho=0$ is satisfied. The (ξ^2,λ) pairs for which $F_{\lambda,\xi}(0)=0$ were obtained by numerical computation and are plotted in Fig. 1 (for $c_1=c_2=\frac{1}{2}$).

Noting that $\lambda\xi=2g^2\zeta/\hbar$ the bound-state wave

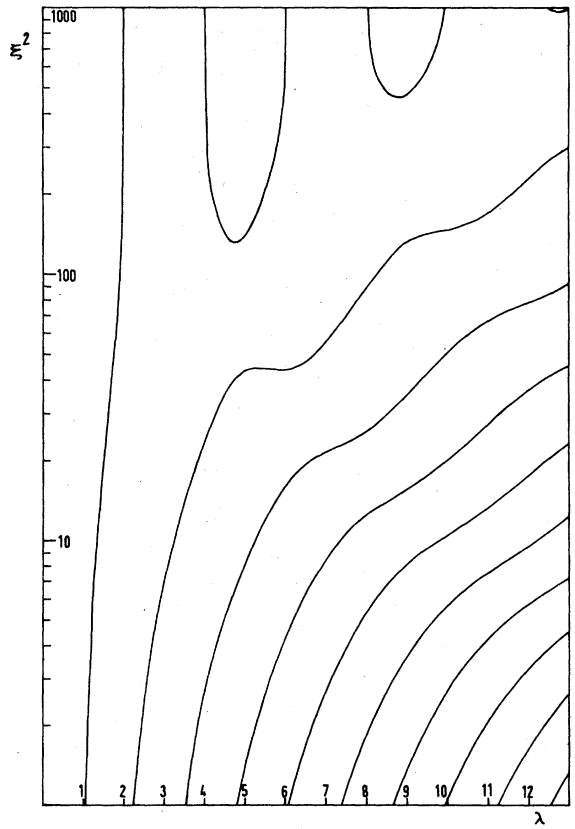

FIG. 1. Zeros of $F_{\lambda,\xi}(0)$ [Eq. (2.8)].

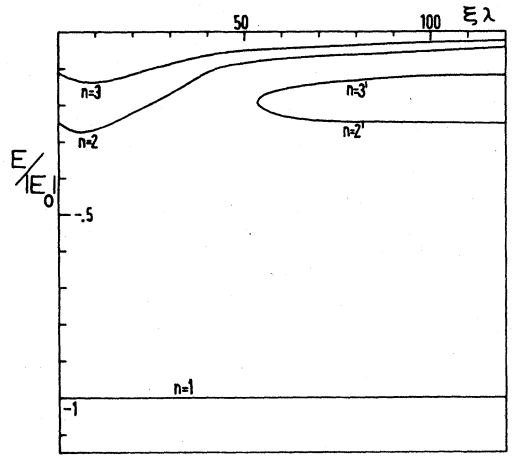

FIG. 2. Radial excitation energy as a function of $\xi\lambda = 2g^2\zeta/\hbar$.

functions for a given set of fixed coupling constants are obtained at the intersections of $\lambda\xi = \text{const}$ lines with the lines of zeros in Fig. 1. The bound-state energies are, up to a constant, the ξ^2 coordinates of these intersections.

At $(\lambda\xi)_1 \simeq 53.2$ one crosses a critical point in the radial excitation level structure, and above this value there are two levels for the principal quantum numbers $n=2$ and 3. This is illustrated in Fig. 2, with all energies being normalized to the same ground-state energy $E_0 = E_{(n=1)}$.

Similarly above $(\lambda\xi)_2 \simeq 186$ the levels from $n=2$ to $n=5$ are doubled and, in general, above a certain $(\lambda\xi)_r$ all levels from $n=2$ to $n=2r+1$ become doubled. At very high $\lambda\xi$ values the $n=2,3,4\ldots$ levels collapse to zero whereas the primed levels $n=2',3',4'\ldots$ tend to pure Coulombic values. This is as one expects on physical grounds because for very high ξ values the nonlocal cosine term in the potential oscillates very rapidly in momentum space and the motion of the particle is determined by the average $1/r$ potential. The most interesting and qualitatively different effects are therefore expected to occur only for small to moderate ($\lesssim 60$)$\lambda\xi$ values.

III. PARABOLIC APPROXIMATION

For small ξ values one may expand the cosine and keep a finite number of terms to obtain useful local approximations to the nonlocal equation (2.4). For the approximation

$$\cos\left[\xi\left(-\frac{d^2}{d\rho^2}+\frac{l(l+1)}{\rho^2}\right)^{1/2}\right] \simeq 1+\frac{\xi^2}{2}\left(\frac{d^2}{d\rho^2}-\frac{l(l+1)}{\rho^2}\right)$$

one obtains

$$\left(\frac{d^2}{d\rho^2}-\frac{l(l+1)}{\rho^2}+\frac{\lambda'}{\rho+a}\right)\tilde{F}_l(\rho) = \tfrac{1}{4}\tilde{F}_l(\rho)\,, \qquad (3.1)$$

where $\lambda' = \lambda + a/4$ and $a = c_2\lambda\xi^2/2$. In this approximation the nonlocal potential is equivalent to a shifted Coulomb potential $1/(\rho+a)$.

For $l=0$ the solution is obtained from (2.8) approximating the cosine in the second integral:

$$\tilde{F}_0(\rho) = \frac{\sqrt{2}}{\pi}\int_0^{\pi/2} d\phi\,\cos\left(\frac{\rho+a}{2}\tan\phi - 2\lambda'\phi\right)\,. \qquad (3.2)$$

In this approximation the solution is therefore $(1/\sqrt{2})K_{2\lambda'}(\frac{1}{2}(\rho+a))$, K being the Bateman function,[2] a particular case of the confluent hypergeometric function.

For $l \neq 0$ the replacement

$$\tilde{F}_l(\phi) = h_l(\phi)\rho^{l+1}$$

yields

$$\rho h'' + 2(l+1)h' + \rho\left(\frac{\lambda'}{\rho+a}-\frac{1}{4}\right)h = 0\,. \qquad (3.3)$$

The bound-state wave functions correspond to solutions satisfying $(h'/\rho)_0 = (\frac{1}{4}-\lambda'/a)h(0)/(2l+3)$ and $h \sim \exp(-\rho/2)$ at infinity. This fairly simple matching problem was solved numerically for $c_2 = \frac{1}{2}$. The allowed (ξ^2,λ) pairs are plotted in Fig. 3, the stability of the numerical algorithm being

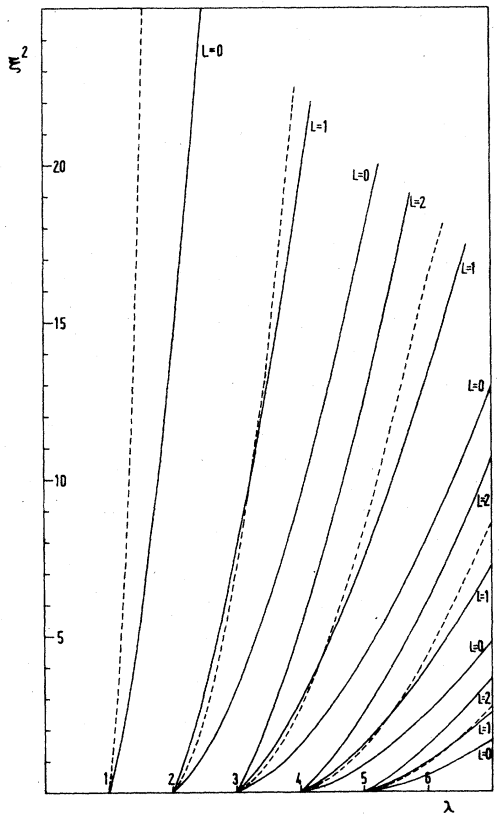

FIG. 3. ξ^2,λ pairs corresponding to bound states of the parabolic approximation, Eq. (3.1).

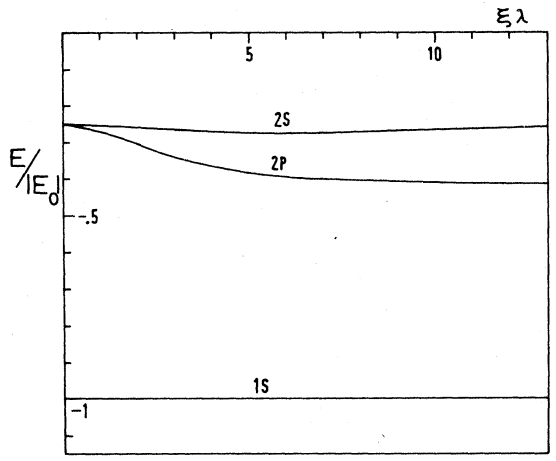

FIG. 4. 2S-2P splitting from the parabolic approximation scaled by the exact radial level energies.

tested through comparison with the analytical solution (3.2) for $l=0$.

The dashed lines in Fig. 3 are the curves corresponding to the exact solution for $l=0$, Eq. (2.8). Comparison of the exact and the approximate $l=0$ curves shows that although they are quantitatively different they have similar shapes. This suggests that a not too unrealistic estimate of the level splittings (for small $\xi\lambda$ values) might be obtained by scaling the splittings of the approximate equation by the exact radial excitation differences, i.e., if $E[nl]$ is the exact energy of the nl level and $\epsilon[nl]$ the corresponding energy of the approximate equation one sets

$$E[2S]-E[2P]\simeq\frac{\epsilon[2S]-\epsilon[2P]}{\epsilon[2S]-\epsilon[1S]}\{E[2S]-E[1S]\}$$

and in general

$$E[nS]-E[nl]\simeq\frac{\epsilon[nS]-\epsilon[nl]}{\epsilon[nS]-\epsilon[(n-1)S]}\{E[nS]-E[(n-1)S]\}.$$

The result of such a calculation for the $2P$ state yields the estimated splittings plotted in Fig. 4, all energies being normalized to the same ground-state energy.

The Coulomb radial wave functions have a simple analytical form, namely a polynomial times $\exp(-\rho/2)$. This is also true for special cases of the approximate solution $\tilde{F}_0(\rho)$, when λ and ξ are such that $2\lambda'=2\lambda+\lambda\xi^2/8$ is an even integer. Then the Bateman function $K_{2\lambda'}$ is the difference of two Laguerre polynomials. Because simple analytical forms may be useful for practical calculations I have listed in the following tables some $1S$ and $2S$ normalized wave functions. The notation is

$$\tilde{f}_0(\rho)=c\sum_n a_n\rho^n\exp(-\rho/2),$$

all functions being normalized to $\int_0^\infty\tilde{f}_0(\rho)d\rho=1$. Also listed is the value $\Phi(0)=[\tilde{f}_0(\rho)/\rho]_{\rho=0}$.

Exact and approximate solutions have (for small $\xi\lambda$) qualitatively similar spectra and for large ρ behave in a similar way. In particular they both display increasing spreading when $\xi\lambda$ grows. However, one anticipates distinct behavior for small ρ values because then large values of α can contribute to the integral transform (2.5) and $1-\xi^2\alpha^2/2$ is no longer a good approximation to $\cos(\xi\alpha)$. The behavior at the origin of the exact S-wave functions shows some unusual features and is discussed in the next section.

IV. WAVE-FUNCTION VALUES AT THE ORIGIN

Let

$$g_{\lambda,\xi}(\phi)=2\lambda\left[c_1\phi+c_2\int_0^\phi\cos\left(\frac{\xi}{2}\tan\phi'\right)d\phi'\right]. \tag{4.1}$$

From Eq. (2.8)

$$\begin{aligned}F_{\lambda,\xi}(\rho)=&\frac{\sqrt{2}}{\pi}\int_0^{\pi/2}\cos\left(\frac{\rho}{2}\tan\phi\right)\cos g_{\lambda,\xi}(\phi)d\phi\\&+\frac{1}{\pi\sqrt{2}}\sin g_{\lambda,\xi}(\pi/2)\int_0^\infty\frac{\sin(\rho\alpha)}{\alpha^2+\frac{1}{4}}d\alpha\\&+\frac{\sqrt{2}}{\pi}\int_0^{\pi/2}\sin\left(\frac{\rho}{2}\tan\phi\right)\\&\times[\sin g_{\lambda,\xi}(\phi)-\sin g_{\lambda,\xi}(\pi/2)]d\phi.\end{aligned} \tag{4.2}$$

TABLE I. 1S wave functions (parabolic approximation).

$\lambda\xi$	c	a_1	a_2	a_3	a_4	a_5	a_6	a_7	$\Phi(0)$
0	0.707 10	1							0.707 10
3.464 10	0.133 63	2	1						0.267 26
5.864 49	0.011 756	16.392 30	8.196 15	1					0.192 70
7.996 36	6.6646×10^{-4}	235.75	117.875	19.035	1				0.157 12
9.954 4	2.7669×10^{-5}	4 896.40	2 448.20	443.56	34.769	1			0.135 48
11.785 2	9.0257×10^{-7}	133 652.67	66 826.33	12 902.95	1 211.242	55.560	1		0.120 63
13.516 9	2.4187×10^{-8}	4 533 902.3	2 266 952.1	455 890.7	47 526.38	2 722.197	81.521	1	0.109 66

TABLE II. 2S wave functions (parabolic approximation).

$\lambda\xi$	c	a_1	a_2	a_3	a_4	a_5	a_6	a_7	$\Phi(0)$
0	0.353 55	−2	1	1					−0.707 107
3.688 86	0.062 97	−4.392 30	−2.196 15	1.221 63	1	1			−0.276 58
6.477 71	5.7641×10^{-3}	−34.881	−17.440 3	−10.030 2	8.655 89		1		−0.201 05
9.043 07	3.4807×10^{-4}	−471.716	−235.858	−434.287	98.304 8	20.3944			−0.164 19
11.446 97	1.5513×10^{-5}	−9 122.56	−4 561.28	−14 520.756	1302.414	449.4258	36.6423	1	−0.141 52
13.724 16	5.4456×10^{-7}	−231 147.94	−115 573.33						−0.125 87

From

$$\int_0^\infty d\alpha \sin(\rho\alpha)/(\alpha^2+\tfrac{1}{4}) = \left[e^{-\rho/2}\overline{\mathrm{Ei}}\left(\frac{\rho}{2}\right) + e^{\rho/2}E_1\left(\frac{\rho}{2}\right)\right]$$

and for (λ,ξ) values for which $F_{\lambda,\xi}(0)=0$ it follows that the leading behavior of $F_{\lambda,\xi}(\rho)$ when $\rho\to 0$ is

$$F_{\lambda,\xi}(\rho) \simeq \frac{1}{\pi\sqrt{2}} \mathrm{sing}_{\lambda,\xi}\left(\frac{\pi}{2}\right)[\rho(1-\gamma) - \rho\ln\rho/2] - \frac{\rho}{2\sqrt{2}} \mathrm{cosg}_{\lambda,\xi}\left(\frac{\pi}{2}\right) + \frac{\rho}{\pi\sqrt{2}} \int_0^{\pi/2} \tan\phi \left[\mathrm{sing}_{\lambda,\xi}(\phi) - \mathrm{sing}_{\lambda,\xi}\left(\frac{\pi}{2}\right)\right] d\phi \,, \tag{4.3}$$

where γ is Euler's constant ($\gamma = 0.577\,215\,6\ldots$). Therefore $F_{\lambda,\xi}(\rho) \sim \alpha\rho - \beta\rho\ln\rho$ and the wave function of the exact S states behaves like $\alpha - \beta\ln\rho$ at the origin.

This $\ln\rho$ behavior at the origin is an intrinsic feature of the nonlocal potential. Referring back to Eq. (2.4) or (2.6) one sees that it arises because $\int d\alpha\, \phi_0(\alpha) = 0$ does not, in general, imply the vanishing of $\int [c_1 + c_2\cos(\xi\alpha)]\phi_0(\alpha) d\alpha$. Then the $1/\rho$ singularity at $\rho = 0$ remains in the equation to be canceled only by the second derivative of $\beta\rho\ln\rho$.

A similar reasoning shows that if, by using asymptotic-freedom arguments, one softens the $1/\rho$ behavior of the potential to $1/\rho\ln\rho$ at short distances, then, as long as the nonlocal term $c_1 + c_2\cos(\ldots)$ remains, the wave function is still infinite at the origin, its leading behavior being in this case $\ln|\ln\rho|$.

In both cases the infinities are sufficiently soft so as not to be physically troublesome. Indeed $r\psi(x) \to 0$ as $r \to 0$ as required by the Hermiticity of the radial momentum and although $\psi(r) \to \infty$, the probability to find the particle in a small sphere of radius R around the origin remains finite and vanishes as $R \to 0$. The infinity, however, precludes the use of the Van Royen-Weisskopf[3] formula in its simple form:

$$\Gamma(V \to l^+ l^-) = |\psi(0)|^2 16\pi\alpha^2 e^2 / M_V{}^2 \,. \tag{4.4}$$

However, one should remember that the application of this formula to the leptonic annihilation of quarkonia corresponds to a highly idealized situation where the mass of the constituents $m_Q \to \infty$ and the wave functions are smooth at the origin. A better estimate should be obtained by replacing $|\psi(0)|^2$ in (4.4) by the average value of $|\psi(x)|^2$ in a sphere of radius $1/m_Q$.[4] Therefore, if $F_{\lambda,\xi}(\rho) \sim \alpha\rho - \beta\rho\ln\rho$ the value that should replace $|\psi(0)|^2$ in Eq. (4.4) is

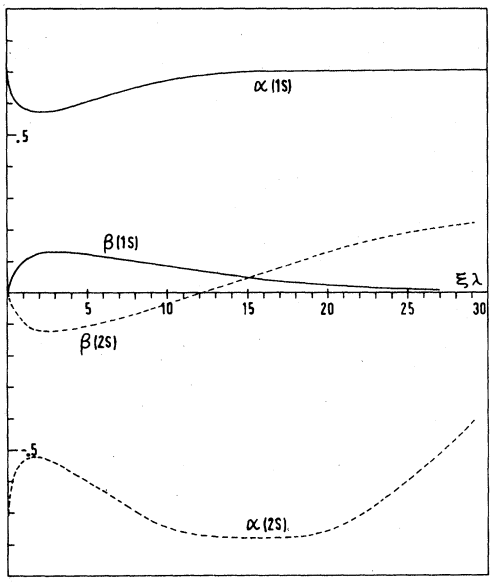

FIG. 5. Coefficients for the behavior of the S states at the origin ($\alpha - \beta \ln\rho$).

$$|\bar{\psi}|^2 = (4m_Q|E|)^{3/2}\left\{\alpha^2 - (2\alpha\beta + \tfrac{2}{3}\beta^2)\left[\ln\left(\frac{4|E|}{m_Q}\right)^{1/2} - \frac{1}{3}\right] + \beta^2 \ln^2\left(\frac{4|E|}{m_Q}\right)^{1/2}\right\}, \quad (4.5)$$

where $|E|$ is, in the notation of (2.3), the binding energy of the state and the reduced mass m has been identified with $m_Q/2$. In Fig. 5 the values of α and β were plotted for normalized $[\int_0^\infty F^2(\rho)d\rho = 1]$ $1S$ and $2S$ wave functions.

V. CONCLUSIONS

I will conclude with some comments concerning the relationship between the results of this study and potential models for quarkonium systems.

With the appropriate choice of the masses and couplings, any potential can accommodate the $1S$-$2S$ splitting; however, factors such as $\alpha_3 = (E_{3S} - E_{2S})/(E_{2S} - E_{1S})$ are peculiar to the nature of the potential. From the level structure in Fig. 2 it is clear that the potential V of Eq. (1.2) cannot by itself accommodate the values $\alpha_3 = 0.6$–0.7 found in the ψ and Υ families. As mentioned before, V should be looked at as a short-to-intermediate-range potential (playing the same role as the Coulomb potential in conventional models) to be supplemented by a long-range potential in phenomenological applications.

We also do not see yet any evidence for phenomena such as the doubling of radial excitations predicted for high $\xi\lambda$ values. In this connection it is worthwhile to point out that the short-range part of the potential is not what is tested by most of the charmonium data and that a precise knowledge of the short-range potential will become increasingly important for the heavier quarkonium families.

For the $2S$-$2P$ splitting parameter $\beta = (E_{2S} - E_{2P})/(E_{2S} - E_{1S})$ one estimates from Fig. 4 $\beta = 0.17$–0.21 in the range $\lambda\xi = 6 - 13$. Comparing with $\beta = 0.28$ for the splitting between the ψ' and the center of gravity of the ^3P_J charmonium levels one concludes that a sizable part of the $2S$-$2P$ splitting might already be due to the short-range potential and not purely to the long-range part as in conventional models.

The main purpose of this paper has been to study in a fairly rigorous manner the nature of the bound states of our non-Abelian replacement for the Coulomb potential. For phenomenological applications, however, one must add a confinement piece,

$$V_{\text{ph}} = -\frac{g^2}{2r}\left\{1 + \cos\left[\xi\left(-\frac{\hbar^2\nabla^2}{m^2}\right)^{1/2}\right]\right\} + \frac{1}{b^2}V_c\,. \quad (5.1)$$

As a first approximation to the study of (5.1) one might use, in the spirit of Ref. 5, a variational method using a set of normalized functions

$$Y_k(r) = (8m|E|k^2)^{1/2}F_{\lambda,\xi}((8m|E|k^2)^{1/2}r)/r \quad (5.2)$$

as trial wave functions, k being the variation parameter to be obtained minimizing the expectation value of the energy for each level separately. Because for moderate $\lambda\xi$ the structure of the levels is nearly Coulombic one may even use as a first approximation Coulomb wave functions to obtain estimates for the k's which are then to be used in the trial functions (5.2). Carrying out this calculation for $V_c = r^2$, r, $\ln(r/r_0)$, with parameters chosen to fit the $1S$ and $2S$ states of $c\bar{c}$ and $b\bar{b}$

TABLE III. k values for $1S$ and $2S$ states of $c\bar{c}$, $b\bar{b}$, and $t\bar{t}$ bound states.

Confinement potential	g^2	$1/b^2$	r_0^2	ψ k_{1S}	ψ k_{2S}	Y k_{1S}	Y k_{2S}	t k_{1S}	t k_{2S}
r^2	0.64	0.03 GeV^3		1.59	3.69	1.06	1.74	1.00	1.08
r	0.52	0.2 GeV^2		2.10	4.61	1.24	2.22	1.03	1.28
$\ln r/r_0$	0.57	0.4 GeV	0.29 GeV^{-2}	1.95	4.39	1.37	2.57	1.13	1.69

bound states, one obtains the corresponding k values for these states and for $t\bar{t}$ bound states (see Table III). The constituent masses used were, respectively, $m_c = 1.32$, 1.33, 1.525, $m_b = 4.86$, 4.78, 4.97, and $m_t = 17$. The $1S$-$2S$ mass splittings obtained for $t\bar{t}$ bound states are 0.99, 1.03, 1.34. The lower values refer to the logarithmic potential and the higher values to the harmonic potential.

[1]R. Vilela Mendes, Nucl. Phys. B161, 283 (1979).
[2]H. Bateman, Trans. Am. Math. Soc. 33, 817 (1931).
[3]R. Van Royen and V. F. Weisskopf, Nuovo Cimento 50A, 617 (1967).
[4]E. C. Poggio and H. J. Schnitzer, Phys. Rev. D 20, 1175 (1979). These authors replace $|\psi(0)|^2$ with $|\psi(r=1/m_Q)|^2$. However in their derivation smoothness of $\psi(x)$ at the origin is again implied. For a singular $\psi(x)$ a probability average over a sphere of radius equal to the Compton wavelength is a more reasonable estimate.
[5]J. Dias de Deus, A. B. Henriques, and J. M. R. Pulido, Z. Phys. C 7, 157 (1981).